Received: 23 July 2018 | Revised and accepted: 19 October 2018
DOI: 10.1002/glia.23563

GLIA
WILEY

RESEARCH ARTICLE

TREM2 triggers microglial density and age-related neuronal loss

Bettina Linnartz-Gerlach[1] | Liviu-Gabriel Bodea[1,2] | Christine Klaus[1] | Aurélien Ginolhac[3] | Rashi Halder[4] | Lasse Sinkkonen[3] | Jochen Walter[5] | Marco Colonna[6] | Harald Neumann[1]

[1]Neural Regeneration, Institute of Reconstructive Neurobiology, University Hospital of Bonn, University of Bonn, Bonn, Germany

[2]Clem Jones Centre for Ageing Dementia Research, Queensland Brain Institute, The University of Queensland, St Lucia, Queensland, Australia

[3]Life Sciences Research Unit, University of Luxembourg, Belvaux, Luxembourg

[4]Luxembourg Centre for Systems Biomedicine, University of Luxembourg, Esch-sur-Alzette, Luxembourg

[5]Department of Neurology, University Bonn, Bonn, Germany

[6]Washington University School of Medicine, Department of Pathology & Immunology, St. Louis, Missouri

Correspondence
Harald Neumann, Neural Regeneration Unit, Institute of Reconstructive Neurobiology, University of Bonn, Sigmund-Freud-Str. 25, 53127 Bonn, Germany,
Email: harald.neumann@uni-bonn.de

Funding information
Deutsche Forschungsgemeinschaft, Grant/Award Numbers: DFG-ImmunoSensation-EXC1023, DFG-SFB704, DFG-LI 2833/1-1; Gemeinnützige Hertie-Stiftung; Innovative Medicines Initiative 2 Joint Undertaking (IMI 2 JU), Grant/Award Number: No 115976 (PHAGO)

Abstract

The microglial triggering receptor expressed on myeloid cells 2 (TREM2) signals via the activatory membrane adaptor molecule TYROBP. Genetic variants or mutations of TREM2 or TYROBP have been linked to inflammatory neurodegenerative diseases associated with aging. The typical aging process goes along with microglial changes and mild neuronal loss, but the exact contribution of TREM2 is still unclear. Aged TREM2 knock-out mice showed decreased age-related neuronal loss in the substantia nigra and the hippocampus. Transcriptomic analysis of the brains of 24 months old TREM2 knock-out mice revealed 211 differentially expressed genes mostly downregulated and associated with complement activation and oxidative stress response pathways. Consistently, 24 months old TREM2 knock-out mice showed lower transcription of microglial (*Aif1* and *Tmem119*), oxidative stress markers (*Inos*, *Cyba*, and *Cybb*) and complement components (*C1qa*, *C1qb*, *C1qc*, *C3*, *C4b*, *Itgam*, and *Itgb2*), decreased microglial numbers and expression of the microglial activation marker Cd68, as well as accumulation of oxidized lipids. Cultured microglia of TREM2 knock-out mice showed reduced phagocytosis and oxidative burst. Thus, microglial TREM2 contributes to age-related microglial changes, phagocytic oxidative burst, and loss of neurons with possible detrimental effects during physiological aging.

KEYWORDS

aging, microglia, neurodegeneration, oxidative stress, TREM2

1 | INTRODUCTION

Triggering receptor expressed on myeloid cells 2 (TREM2) is an innate immune receptor that recognizes a broad spectrum of polyanionic molecules including lipopolysaccharides of bacteria, sulfated glycosaminoglycans, and phospholipids (Cannon, O'Driscoll, & Litman, 2012; Daws et al., 2003; Wang et al., 2015). TREM2 is expressed on microglia, resident self-renewing mononuclear phagocytes of the brain that are derived from embryonic hematopoiesis (Kierdorf et al., 2013). Upon stimulation, TREM2 on microglia associates with the adaptor protein TYROBP/DAP12 leading to a widespread immunoreceptor tyrosine-based activation motif (ITAM)-mediated signaling. This can

result in proliferation, survival, phagocytosis, phagocytic oxidative burst with production of reactive oxygen species (ROS), as well as pro- and anti-inflammatory cytokine expression (Charles et al., 2008; Otero et al., 2012; Takahashi, Rochford, & Neumann, 2005; Wang et al., 2015).

Loss-of-function mutations of TREM2 and TYROBP have been linked to development of Nasu–Hakola disease (NHD; Paloneva et al., 2000, 2002), an inflammatory degenerative disease of the brain and bone, leading to premature dementia and death (Bianchin, Martin, de Souza, de Oliveira, & Rieder, 2010). Rare variants of TREM2 are associated with increased risk of developing Alzheimer's disease (AD; Guerreiro et al., 2013; Jonsson et al., 2013). Most TREM2 mutations found in AD risk variants are heterozygous mutations that impact the binding of TREM2 ligands (Kober et al., 2016) or the shedding of the extracellular domains, also containing the TREM2 ligand binding site (Schlepckow et al., 2017; Thornton et al., 2017).

Since TREM2 mutations are associated with neurodegenerative diseases, aged homozygous TREM2 knock-out (KO) mice could be an animal model for NHD and might give insight into the pathomechanism of AD. Therefore, we analyzed the neuroinflammatory and neurodegenerative phenotype in 24 months old TREM2 KO mice.

Here we show that TREM2 KO mice are protected against age-related inflammatory changes, accumulation of oxidized lipids and loss of neuronal structures.

2 | MATERIALS AND METHODS

2.1 | Animals

All animal experiments have been approved by the authors' institutional review boards and by the local government and have been conducted according to the principles expressed in the Helsinki Declaration. We used male B6.129P2-TREM2^{tm1cln} mice (referred to hereafter as TREM2 KO mice; Turnbull et al., 2006) and their corresponding wild-type (wt) littermates as controls.

2.2 | RNA sequencing, pathway enrichment, and gene transcript analyses

Half brains were collected after PBS perfusion of mice and immediately homogenized in 1 ml QIAzol Lysis reagent (Qiagen, Germany) for two times 3 min at 50 Hz using a Tissue Lyser LT (Qiagen, Germany) and stainless steel beads (mean diameter: 7 mm, Qiagen, Germany). Total RNA was extracted using the spin column protocol of the RNeasy® Mini Kit (Qiagen, Germany) according to the manufacturer's protocol. The RNA concentration was measured using a Nanodrop system (NanoDrop 200c, Thermo Fisher Scientific, Waltham, MA) and diluted to 100 ng/µl. RNA integrity was assessed using 2100 Bioanalyzer (Agilent, Santa Clara, CA). Transcripts were analyzed by RNA sequencing and pathway enrichment as described in Supporting information Methods. For reverse transcription (RT) of isolated RNA, Superscript® III Reverse Transcriptase (Invitrogen, Germany) and random hexamer oligonucleotides (Roche, Germany) were used following the manufacturers' protocol for SuperScript First-Strand Synthesis (Invitrogen, Germany). As controls reactions without addition of cDNA were performed. The cDNA concentration was measured with a Nanodrop system (NanoDrop 200c, Thermo Fisher Scientific). sqRT PCR with specific oligonucleotides (for sequences see *SI Methods*) was performed with SYBR GreenER qPCRSuperMix Universal (Invitrogen, Germany) using the Eppendorf ep gradient S Mastercycler®. Regulation of the housekeeping genes *glyceraldehyde-3-phosphate dehydrogenase (Gapdh)*, *beta-Actin*, *18S*, and *Rpl13a* were investigated in 24 months old TREM2 KO versus wt animals (Supporting Information Figure S1). The Vulcano Plot (Supporting Information Figure S1A) as well as the comparison of the cycle threshold (ct; Supporting Information Figure S1B) demonstrated that none of the investigated housekeeping genes was regulated. Thus, gene transcripts of the housekeeping gene GAPDH were used for normalization. Amplification specificity was confirmed by the analysis of the melting curves. Quantification using the ΔΔCt method was carried out.

2.3 | Immunohistochemistry

Mouse half brain tissues of PBS-perfused mice were immersed in 4% paraformaldehyde (PFA, Sigma, Germany) for 24 hr, followed by 30% sucrose (Sigma, Germany) supplemented with 0.1% sodium azide (Sigma, Germany) until processed into frozen sections. The hemisphere was embedded in O.C.T.™ Compound, Tissue Tek® (Sakura, Torrance, CA), cut into 20 µm coronal sections and stored at −20°C before staining.

For analysis of neurons or oxidized lipids, sections were blocked and permeabilized using 10% bovine serum albumin (BSA, Sigma, Germany), 5% normal goat serum (Invitrogen) and 0.2% Triton X-100 (Sigma, Germany) in PBS followed by the primary antibodies rabbit-anti-tyrosine hydroxylase (TH; 1:500; Sigma, Germany) and anti-NeuN (1:500; Millipore, Germany) or mouse-anti-4-hydroxynonenal (Hne, 1:15; Abcam, United Kingdom) in blocking solution for 2 hr at room temperature. For microglial analysis, sections were blocked and permeabilized using 10% BSA and 0.25% TritonX-100 in PBS followed by the primary antibodies rabbit-anti-ionized calcium-binding adapter molecule 1 (Iba1, 1:500; Wako, Japan) and rat-anti-mouse Cd68 (1:500; Bio-Rad, Germany) in incubation solution (IS; 5% BSA and 0.05% TritonX-100 in PBS) overnight at 4°C. For synapse analysis, sections were blocked and permeabilized using 2% BSA and 0.2% TritonX-100 in PBS followed by the primary antibodies mouse-anti-mouse postsynaptic density 95 (PSD95; 1:200; Thermo Fisher Scientific) and rabbit-anti-mouse vesicular glutamate transporter 1 (vGlut1; 1:500; Synaptic Systems GmbH; Germany) in diluent solution (DS; 0.5% BSA and 0.05% TritonX-100 in PBS) for 3 days at 4°C. After three washing steps in 1× PBS for analysis of neurons, oxidized lipids, and synapses or in IS for microglial analysis, the sections were incubated in the corresponding Cy3- or Alexa488-coupled secondary antibodies (1:200 or 1:500 [neurons, oxidized lipids]/1:400 [microglia], respectively; Jackson ImmunoResearch Laboratories, United Kingdom) in blocking solution for analysis of neurons and oxidized lipids or IS for microglial analysis for 2 hr at room temperature or overnight at 4°C in DS for synapse analysis. After two washing steps with 1x PBS, nuclei of cells were labeled with 4′,6-diamidino-2-phenylindole (DAPI, 1:10,000; Sigma, Germany) for 30 s followed by another washing step

with 1× PBS. Sections were embedded with Moviol (Sigma, Germany) or (Aqua-)Polymount (Polysciences Inc, Warrington, PA) and stored at 4°C. Images were taken with ApoTome microscope (AxioImager.Z1) equipped with AxioVisio imaging software (both Zeiss, Germany) for analysis of neurons. For analysis of oxidized lipids, microglia and synapses images were acquired with a confocal microscope (Fluoview1000) equipped with FluoView imaging software (both Olympus, Germany) and 3D reconstruction was performed.

All number-coded images were analyzed by a blinded investigator using the ImageJ software (NIH, MBF, Bethesda, MD). The levels were defined according to the mouse brain atlas of Paxinos & Franklin. For quantification of neuronal density, in total three matching levels per animal were analyzed (Bregma −2.92 mm, −3.52 mm and – 3.64 mm for substantia nigra *pars compacta* [SN*pc*] and Bregma −2.30 mm to −2.46 mm, −2.92 mm, −3.4 mm for hippocampal CA3). The SN*pc* was encircled based on the TH-positive immunostaining and the number of NeuN-positive cells in the selected area was counted. The cell number was divided by the selected area. Moreover, for analysis of the width, different points of the selected CA3 region (pyramidal cell layer as indicated in Figure 1a) as well as of the dentate gyrus (DG) were measured and the mean was calculated. For analysis of oxidized lipids, z-stacks of the 4-Hne stained hippocampus and the SN *pars reticulate* (SN*pr*) were taken at the Bregma level −2.94 mm to −2.98 mm and the intensity per area was calculated and the background was subtracted. For quantification of microglia z-stacks of the SN*pr* at Bregma level −2.88 mm to −2.9 mm were taken. The intensity of Iba1 as well as Cd68 per area was measured and background intensity was subtracted. Additionally, the number of Iba1/DAPI-double positive cells was counted, the soma area was measured according to the Iba1 staining of 10 cells in each picture and the mean value was calculated. Soma intensities of Iba1 and Cd68 were measured in the ten cells encircled for soma area and the corresponding background intensities were subtracted for each soma. For quantification of synapses, two z-stacks were taken of the hippocampus in-between the DG region at Bregma level −2.3 mm to −2.5 mm. The quantification was carried out using the Puncta Analyzer plugin for ImageJ according to Ippolito and Eroglu with a rolling ball radius of 50 and the minimum puncta size of four pixels (Ippolito & Eroglu, 2010). The same settings for the analysis were used for all images.

2.4 | Lipid peroxidation (MDA) assay kit

Brain regions (hippocampus and midbrain) were directly prepared after PBS perfusion of the mice, shock-frozen in liquid nitrogen and stored in −150°C for 1–2 days, before using for the malondialdehyde (MDA) assay kit (Sigma, Germany) that was performed according to manufacturers' protocol. The absorbance of the samples was measured at 532 nm with the EnVision 2104 Multilabel Plate Reader (Perkin Elmer, Waltham, MA).

2.5 | Primary microglia preparation

Primary microglial cultures were prepared from TREM2 wt or KO mice and cultured according to an established protocol (Napoli, Kierdorf, & Neumann, 2009). Primary microglia were cultured in serum-free medium consisting of Dulbecco's Modified Eagle's Medium (DMEM)/F12 supplemented with 1% N2 supplement, 1% L-glutamine and 1% penicillin/streptomycin (all Invitrogen, Gibco, Germany) for 24 hr before using for phagocytosis assay or dihydroethidium (DHE) staining.

2.6 | Phagocytosis assay

Beads phagocytosis assay was performed according to an established protocol (Beutner, Roy, Linnartz, Napoli, & Neumann, 2010). To analyze the phagocytosis of inactivated, pHrodo-labeled bacteria (pHrodo™ Red BioParticles®, *Staphylococcus aureus*, Molecular Probes, Eugene, OR) primary microglia were incubated with 1 mg/ml pHrodo-inactivated bacteria for 2 hr at 37°C, 5% CO_2. Cells were washed with PBS, fixed with 4% PFA containing 0.25% glutaraldehyde (Sigma, Germany), images were taken with a confocal microscope equipped with FluoView imaging software and analyzed using ImageJ software. pHrodo intensity per picture of five pictures per condition per experiment was calculated and background intensity was subtracted.

2.7 | Superoxide detection by DHE staining

Neural necrotic debris has been prepared by incubating ARPE-19 cells (#ATCC-CRL-2302, ATCC, Germany) in PBS for 1 hr at 56°C. Cells were treated for 15 min either with 5 μg/μl debris or 1 μg/μl inactivated bacteria (unlabeled BioParticles ®, *Staphylococcus aureus*, Molecular Probes). Cells were pre-incubated with superoxide dismutase-1 (SOD-1; 40 μg/ml; Serva, Germany) or trolox (80 μM; Cayman, Germany) as indicated before the treatment with inactivated bacteria. Detection of superoxide was carried out according to an established protocol (Claude, Linnartz-Gerlach, Kudin, Kunz, & Neumann, 2013). SOD-1 (debris: 20 μg/ml; inactivated bacteria: 40 μg/ml) or Trolox (debris: 40 μM; inactivated bacteria: 80 μM) were added as indicated.

2.8 | Statistical analysis

Data of at least three independent experiments were normalized to 3 months old wt mice or to wt primary microglia. Data with one variable were analyzed by unpaired Student's *t* test (2 groups) or by ANOVA followed by post hoc Bonferroni correction (>2 groups) using SPSS computer software (IBM Corporation, Germany). Data with more than one variable were analyzed by multiple linear regression including an interaction term followed by a pairwise comparison with LSD-post hoc correction using STATA®/IC computer software (StataCorp, College Station, TX). The Breusch–Pagan/Cook–Weisberg test for heteroscedasticity was performed to assess the equality of variances in the linear model. If variances were significantly different, a robust linear model including an interaction term was chosen for further analysis.

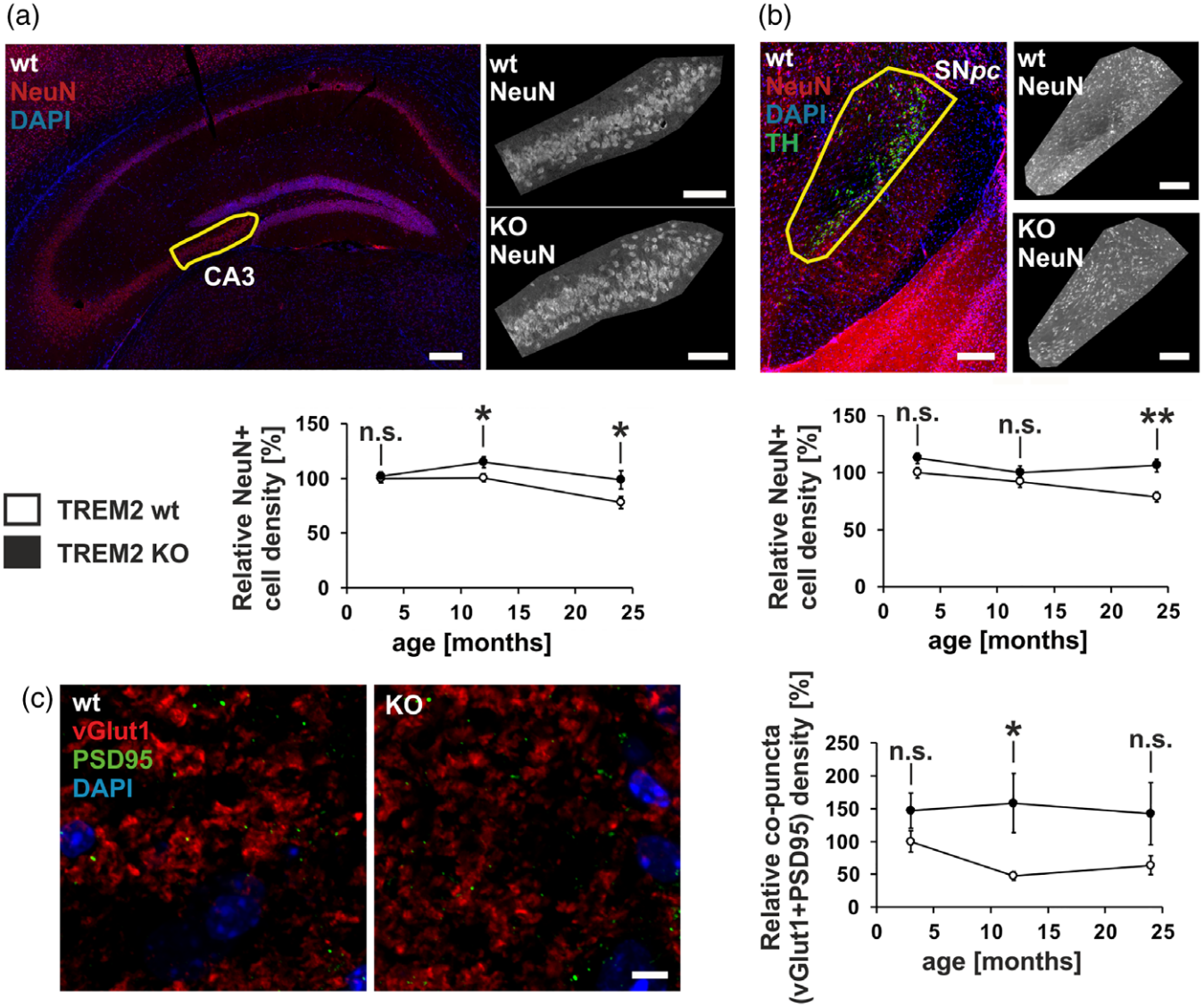

FIGURE 1 Less age-related neuronal loss in TREM2 KO mice. a,b *Up*— Representative images of neuronal nuclei (NeuN, red) and 4′,6-diamidino-2-phenylindole (DAPI, blue) staining in the hippocampus (a) and of NeuN, DAPI and tyrosine hydroxylase (TH, green) in the substantia nigra *pars compacta* (SN*pc*; b) of 24 months old TREM2 wild-type (wt) and knock-out (KO) mice. Quantification was carried out in the encircled area. Scale bar: 200 μm, higher magnifications of hippocampus: 100 μm, Bregma level: Hippocampus: −2.4 mm, SN*pc*: −2.92 mm. *Down*—quantification of NeuN-positive cell density of 3, 12, and 24 months old TREM2 wt versus KO mice in the hippocampal CA3 region (a) and in the SN*pc* (b) showed a higher NeuN-positive cell density in 24 months old TREM2 KO mice. (c) *Left*—representative z-stack images of vesicular glutamate transporter 1 (vGlut1, red) and postsynaptic density protein 95 (PSD95, green) positive structures in-between the dentate gyrus in 24 months old TREM2 wt versus KO mice. Bregma level: −2.30 to −2.50 mm. Scale bar: 5 μm. *Right*—quantification of synapses (co-puncta density) in 3, 12, and 24 months old TREM2 wt versus KO mice revealed a higher synaptic density in TREM2 KO mice. Data are presented as mean ± *SEM* (*n* = 6–12 mice per group. * $p \leq .05$; ** $p \leq .01$; n.s. not significant)

3 | RESULTS

3.1 | Decreased age-related neuronal loss in TREM2 KO mice

To investigate the role of TREM2 in brain aging, neuronal loss was analyzed in two selected brain regions, the SN and the hippocampus. The neurons in the SN*pc* are susceptible to oxidative stress, a process occurring in the aging brain. The CA3 region of the hippocampus is involved in memory processes and is susceptible to neurodegeneration. NeuN-positive cells were counted per selected area as indicated in Figure 1a,b (*up*) and the relative cell density was quantified in 3, 12 and 24 months old TREM2 wt versus KO mice (Figure 1a,b [*down*]). In wt animals, the relative neuronal density decreased with age in both brain regions (3 months versus 24 months: $p = .002$ for hippocampus and $p = .005$ for SN*pc*). In contrast, in the TREM2 KO mice, the relative numbers of NeuN-positive cells were neither decreasing in the hippocampus (3 months vs. 24 months: $p = .624$) nor in the SN*pc* (3 months vs. 24 months: $p = .431$). Thus, the number of NeuN-positive cells was generally higher in TREM2 KO mice (genotype-specific difference: $p = .0016$ in hippocampus and $p = .0002$ in SN*pc*), especially at 24 months of age (hippocampus: wt 78.06 ± 5.5%, KO 98.74 ± 8.3%, $p = .011$; SN*pc* wt 78.71 ± 4.26%, KO 106.6 ± 5.58%, $p = .002$). To investigate changes in tissue

morphology due to different neuronal densities, the width of the DG as well as of the CA3 region was analyzed and found to be increased in aged TREM2 KO mice compared to wt mice (Supporting Information Figure S2; genotype-specific difference in CA3: $p < .0001$). To investigate alterations of neuronal-specific structures, the synaptic density in the hippocampus was analyzed. Coronal sections were stained with antibodies for glutamatergic pre- and post-synapses (Figure 1c, *left*) and the co-puncta density was quantified (Figure 1c, *right*). In the TREM2 KO mice, the co-puncta density was higher compared to the wt animals (genotype-specific difference: $p = .0022$).

Taken together, less age-related neuronal loss accompanied by increased synaptic density was detected in TREM2 KO mice compared to wt littermates.

3.2 | Diminished activation of complement and oxidative stress pathways in aged TREM2 KO mice

To better understand the molecular mechanisms leading to less neuronal loss in aged TREM2 KO mice compared to wt littermates, transcriptomic analysis of 24 months old brains was performed. In total, 211 genes were found to be differentially expressed (DE) above 0.5-fold on $\log_2$-scale with a false discovery rate (FDR) < 0.05 (Supporting Information Figure S3a). The DE genes included genes of the complement system (e.g., *Itgb2* [cd18], *C4b*, *C3*), genes involved in an oxidative stress response (e.g., *Cybb*, *Inos*), and microglial markers (e.g., *Cd68*, *Tyrobp*). Interestingly, the before mentioned genes are all downregulated in TREM2 KO mice. An Ingenuity Pathway Analysis® (IPA) using these 211 DE genes revealed as top enriched canonical pathways TREM1 signaling, complement system and production of nitric oxide and ROS in macrophages, with most of the genes downregulated (Supporting Information Figure S3a,b). The top five molecular and cellular functions are cell-to-cell signaling and interaction, cellular function and maintenance, cellular movement, protein synthesis, and cellular development (Supporting Information Figure S3c). The top six predicted upstream regulators from the IPA (Interferon γ [Ifnγ], Tumor necrosis factor α [Tnfα], Interleukin 4 [Il4], Il-1β, Il6, and Ifnα) are all predicted to be inhibited in the 24 months old TREM2 KO mice compared to wt littermates (Supporting Information Figure S3d).

Thus, data indicate that the innate immune system of the brains of aged TREM2 KO mice is in a less activated state as indicated by the lower expression of genes involved in the innate immune, complement, and oxidative stress response pathways.

3.3 | Decreased age-related expression of microglial markers and pro-inflammatory cytokines in TREM2 KO mice

To confirm the lower activated innate immune system state in the brains of TREM2 KO mice, the resident immune cells of the brain, the microglia, were investigated. The transcription levels of the microglial markers allograft inflammatory factor 1 (*Aif1*, the iba1 encoding gene) and the transmembrane protein 119 (*Tmem119*) were lower in TREM2 KO mice compared to wt littermates (Figure 2a). The multiple linear regression model revealed genotype-specific differences for both markers (*Aif1* $p = .0045$; *Tmem119* $p = .0094$). The reduced transcription is especially detectable for *Aif1* (wt 0.78 ± 0.1 FC, KO 0.38 ± 0.05 FC, $p = .001$) at 24 months of age. To check whether changes can also be observed on the protein level, coronal sections were stained for Iba1 to analyze the number of microglia. The number of Iba1-positive cells was lower in TREM2 KO mice compared to wt littermates at every investigated time point (Figure 2b *left*; genotype-specific difference: $p = .0012$). Especially at 24 months of age, the relative number of Iba1-positive cells was lower in the TREM2 KO mice compared to wt littermate controls (Figure 2b, *left*; wt 85.87 ± 11.32%, KO 47.57 ± 5.66%, $p = .003$). Additionally, at this age, the relative Iba1 intensity per area (wt 28.1 ± 8.07%, KO 12.25 ± 2.2%) showed a tendency to be lower in TREM2 KO mice ($p = .109$; Figure 2b, *right*). In line with lower microglial numbers, the transcription levels of the pro-inflammatory cytokines *Tnfα* and *Il-1β* were less increased in the TREM2 KO mice (genotype-specific differences: $p < .0001$ for both cytokines; Figure 2c). Especially at 24 months of age, the differences were obvious (*Tnfα* wt 3.82 ± 0.32 FC, KO 1.65 ± 0.19 FC, $p < .001$; *Il-1β* wt 1.27 ± 0.11 FC, KO 0.4 ± 0.04 FC, $p < .001$).

Thus, loss of TREM2 results in reduced numbers of microglia accompanied by lower levels of pro-inflammatory cytokines.

3.4 | Less production of nitric oxide and reactive oxygen species and reduced signs of age-related oxidation in TREM2 KO mice

Oxidative damage is a hallmark occurring in aging phagocytes and the aging brain. Our transcriptomic data indicate differences in the brains of 24 months old TREM2 KO mice and wt littermates, with genes encoding for the proteins involved in the pathways of NO production by inducible NO synthases (iNOS) and superoxide production by nicotinamide adenine dinucleotide phosphate (NADPH) oxidase, or their upstream regulators, being DE or predicted to be affected (Figure 3a). Moreover, all regulated genes are less expressed in the 24 months old TREM2 KO mice and the upstream regulators are predicted to be inhibited, indicating less oxidative stress responses in TREM2 KO mice. To confirm the RNAseq data, transcription levels of oxidative stress markers were analyzed (Figure 3b). The oxidative stress markers were less transcribed in 24 months old TREM2 KO mice (*Inos* wt 0.97 ± 0.06 FC, KO 0.61 ± 0.08 FC, $p = .014$; *Cyba* wt 0.22 ± 0.01 FC, KO 0.12 ± 0.01 FC, $p < .001$; *Cybb* wt 1.29 ± 0.15 FC, KO 0.96 ± 0.05 FC, $p = .038$). Lipid peroxidation is, among others, a consequence of oxidative stress. The 4-Hne is an α,β-unsaturated hydroxyalkenal produced by lipid peroxidation. Since oxidative stress responses are reduced in 24 months old TREM2 KO mice, we investigated whether the detection of oxidized lipids is also changed. Therefore, we stained coronal slices for 4-Hne and investigated the staining intensity in the hippocampus (Figure 3c, *left*) and the SN*pr* (Figure 3c, *right*). The relative 4-Hne intensity per area increased with age in wt mice especially in the hippocampus (Figure 3c, *left*; 3 months vs. 24 months: $p < .001$). In the TREM2 KO mice however, the relative 4-Hne intensity per area was increasing less in the hippocampus (3 months vs. 24 months: $p = .01$; genotype-specific differences: $p < .0001$) and was quite stable with age in the SN*pr* (3 months vs. 24 months: $p = .726$; genotype-specific difference: $p = .0185$). Especially

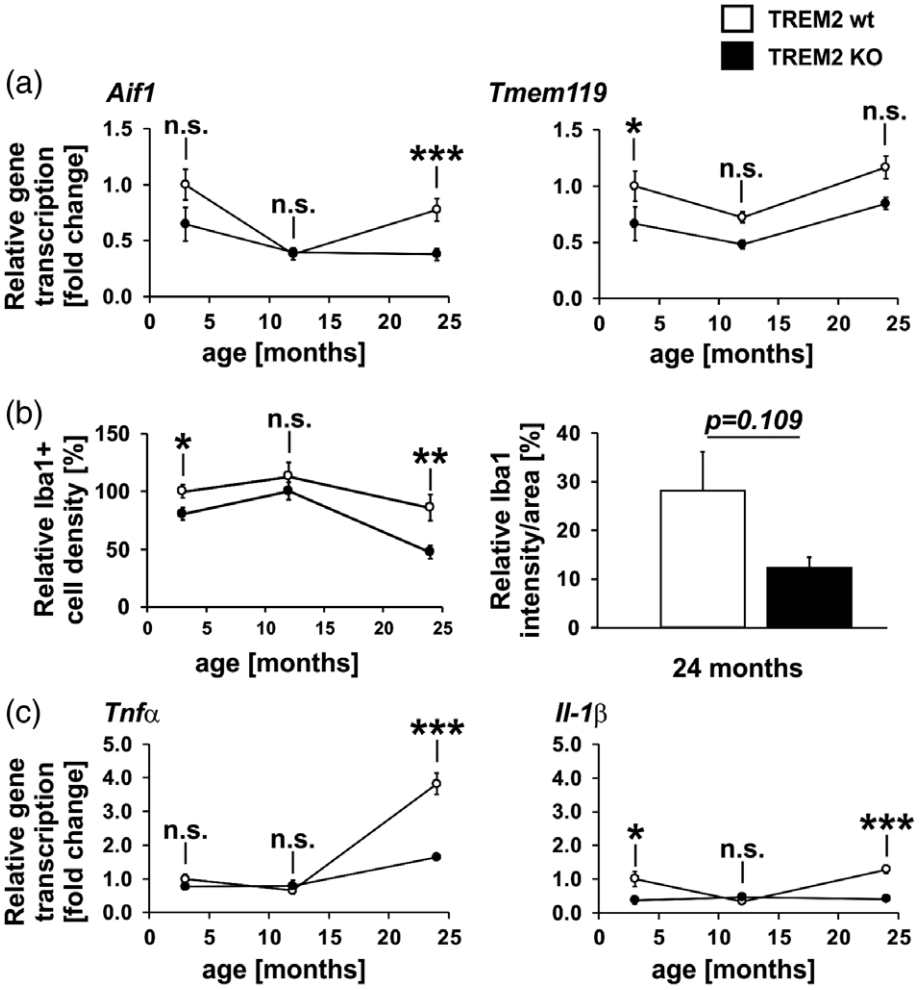

FIGURE 2 Less age-related expression of microglial markers and pro-inflammatory cytokines in TREM2 KO mice. (a) Semi-quantitative real-time (sqRT) PCR of microglial markers in half brains of 3, 12, and 24 months old TREM2 wt and KO mice. At 24 months of age transcription of *aif1* (allograft inflammatory factor 1) and *tmem119* was lower in TREM2 KO mice. *Gapdh* was used as internal loading control. (b) *Left*—quantification of the numbers of Iba1/DAPI double positive cells in the substantia nigra *pars reticulata* (SN*pr*) showed especially at 24 months of age lower amounts of cells per area in TREM2 KO mice. *Right*—quantification of the Iba1 staining intensity per area in the SN*pr* revealed a tendency to lower Iba1 staining intensity in 24 months old TREM2 KO mice. (c) SqRT PCR of pro-inflammatory cytokines demonstrated lower transcription levels of *Tnfα* and *Il-1β* in TREM2 KO mice. *Gapdh* was used as internal loading control. Data are presented as mean + *SEM* or mean ± *SEM* (*n* = 5–12 mice per group; **p* ≤ .05; ***p* ≤ .01; *** *p* ≤ .001; n.s. not significant)

at 24 months of age the relative 4-Hne intensity per area was lower in the hippocampus (wt 180.1 ± 16.71%, KO 119.25 ± 13.84%, $p = .006$) and the SN*pr* (wt 130.9 ± 10.92%, KO 84.4 ± 8.98%, $p = .039$) of TREM2 KO mice. Moreover, lipid peroxidation was also measured via MDA assay in the whole hippocampus (Figure 3d, *left*) and the midbrain (Figure 3d, *right*) of 3 and 12 months old animals. The level of lipid peroxidation was generally lower in TREM2 KO mice compared to wt littermates (Figure 3d; genotype-specific differences: $p = .0142$ [hippocampus] and $p = .0011$ [midbrain]). Especially at 3 months of age, the relative MDA concentration per tissue weight was lower in the hippocampus (wt 100 ± 4.85%, KO 64.36 ± 13.04%, $p = .015$) and the midbrain (wt 100 ± 7.32%, KO 59.91 ± 12.17%, $p = .007$) of TREM2 KO mice. To investigate the microglial oxidative stress responses in more detail, we prepared microglial cultures out of newborn TREM2 KO mice and wt littermates and investigated the production of ROS. Therefore, primary microglia were either treated with necrotic neural debris (Figure 3e) or inactivated bacteria (Figure 3f) and stained with DHE to detect intracellular ROS production. In wt primary microglia, the relative DHE intensity per cell was increased after feeding with debris (from 100 ± 3.12% to 125.99 ± 6.26% after treatment, $p = .007$) and inactivated bacteria (from 100 ± 2.43% to 203.18 ± 12.41% after treatment, $p < .0001$). The superoxide scavengers SOD1 or trolox completely prevented the oxidative burst induced by debris (92.3 ± 3.87%, $p < .001$ vs. debris treatment and 100.69 ± 3.99%, $p = .019$ vs. debris treatment, respectively) or partially prevented the oxidative burst induced by inactivated bacteria (158.28 ± 12.43%, $p = .019$ vs. inactivated bacteria treatment and 167.53 ± 8.78%, $p = .186$ vs. inactivated bacteria treatment, respectively). No increase in ROS production was detectable after treatment of TREM2 KO primary microglia with necrotic neural debris (untreated 90.84 ± 4.46%, $p < .001$; debris treated 94.3 ± 5.72%, $p = .001$; debris+SOD1 treated 95.35 ± 6.2%, $p = .001$; debris+trolox treated 95.06 ± 5.96%, $p = .001$; *p* values versus wt debris treated) or less increased after

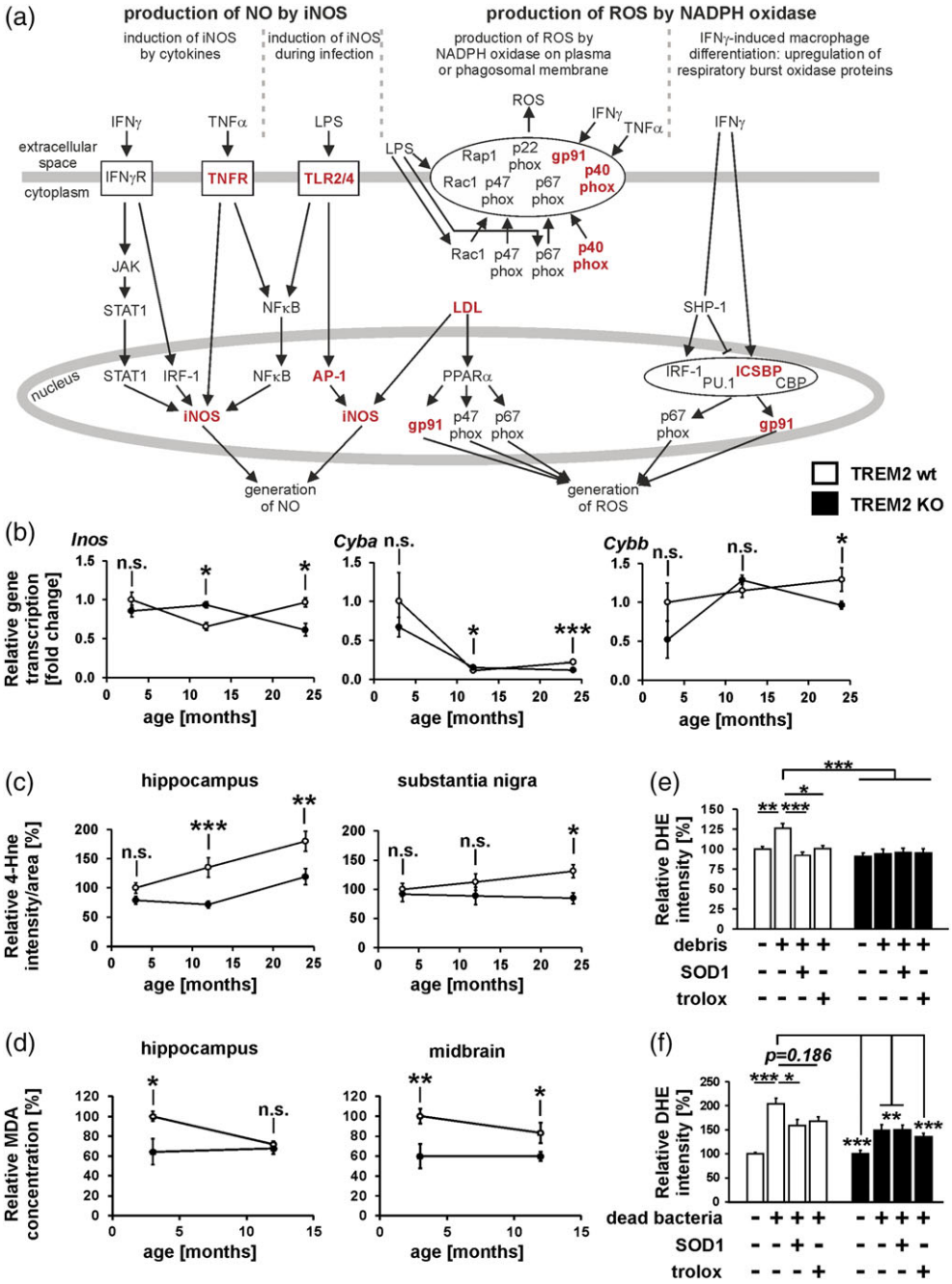

FIGURE 3 Less production of nitric oxide and reactive oxygen species and reduced signs of age-related oxidation in TREM2 KO mice. (a) The pathways of the production of nitric oxide (NO) by inducible NO synthase (iNOS) and reactive oxygen species (ROS) by NADPH oxidase are less activated in 24 months old TREM2 knock-out (KO) animals as revealed by RNA-seq. Significantly down-regulated genes are shown in red and bold. Protein names corresponding to differentially expressed (DE) genes are shown. Ingenuity pathway analysis was performed on significantly DE genes (FC > 0.5, FDR < 0.05). (b) Semi-quantitative real-time PCR of oxidative stress markers in half brain of 3, 12, and 24 months old TREM2 wild-type (wt) and KO. At 24 months of age, transcription of *Inos*, *Cyba*, and *Cybb* was lower in TREM2 KO mice. *Gapdh* was used as internal loading control. (c) Quantification of 4-hydroxynonenal (4-Hne) staining intensity per area in the hippocampus (*left)* and substantia nigra (SN) *pars reticulata* (*right*) showed less (hippocampus) or no (SN) age-related increase of oxidized lipids in 12 and 24 months old TREM2 KO mice. (d) Relative malondialdehyde (MDA) concentrations of 3 and 12 months old TREM2 KO mice were lower in the hippocampus (*left*) and midbrain (*right*). (e,f) Analysis of oxidative stress response in primary microglia obtained from TREM2 wt and KO mice. Quantification of levels of superoxide production after necrotic neural debris feeding (e) or inactivated bacteria treatment (f) as determined by DHE staining intensity showed increased superoxide production in primary wt microglia. The increase was completely (e) or partially (f) antagonized by superoxide dismutase 1 (SOD1) or trolox. In primary TREM2 KO microglia, no (e) or less (f) significant increase in superoxide production was observed after treatment. Data are presented as mean + *SEM* or mean ± *SEM* (n = 6–12 per group (b–d) and n = 4 independent culture preparations (e,f). *$p \le .05$, **$p \le .01$, ***$p \le .001$, n.s. not significant)

treatment with inactivated bacteria (untreated 99.86 ± 7.11%, $p < .001$; inactivated bacteria treated 150.58 ± 9.29%, $p = .002$; inactivated bacteria+SOD1 treated 149.76 ± 9.86%, $p = .002$; inactivated bacteria+trolox treated 135.61 ± 6.75%, $p < .0001$; p values versus wt inactivated bacteria treated).

Thus, lower levels of oxidative stress markers and lipid peroxidation in aged TREM2 KO mice and a lower oxidative burst of TREM2 KO microglia support the data of the RNA-seq analysis and the sqRT PCR hinting toward a reduced oxidative stress response in TREM2 KO animals.

3.5 | Less age-related increase in complement factors in TREM2 KO mice

The complement system is involved in synaptic pruning and the removal of unwanted structures during development, homeostasis, and neurodegeneration via microglial complement-mediated phagocytosis. RNA-seq data identified several DE genes encoding for proteins involved in the different complement cascades (Figure 4a). To validate the RNA-seq results, we performed sqRT PCR to investigate changes in the transcription levels of the complement components *C1qa*, *C1qb*, *C1qc*, *C3*, *C4b*, *Itgam*, and *Itgb2*. Most of the complement markers stayed stable over time in TREM2 KO mice, while some increased with age in the wt littermates (Figure 4b; genotype-specific differences: *C1qa* $p = .0125$; *C1qb* $p = .0982$; *C1qc* $p = .0274$; *C3* $p = .0685$; *C4* $p = .0176$; *Itgam* $p = .0013$; *Itgb2* $p = .0002$). Importantly, in 24 months old animals, all investigated complement components were less transcribed in TREM2 KO mice than in wt littermates (Figure 4b; *C1qa* wt 1.27 ± 0.08 FC, KO 0.8 ± 0.09 FC, $p = .029$; *C1qb* wt 0.72 ± 0.08 FC, KO 0.38 ± 0.05 FC, $p < .001$; *C1qc* wt 4.22 ± 0.35 FC, KO 2.73 ± 0.1 FC, $p = .001$; *C3* wt 1.96 ± 0.18 FC, KO 0.96 ± 0.11 FC, $p = .005$; *C4b* wt 5.41 ± 0.93 FC, KO 2.92 ± 0.29 FC, $p = .012$; *Itgam* wt 0.73 ± 0.05 FC, KO 0.53 ± 0.05 FC, $p = .011$; *Itgb2* wt 2.22 ± 0.17 FC, KO 1.43 ± 0.03 FC, $p < .001$).

Data show that the different gene transcripts of the complement cascades are less upregulated during aging in the TREM2 KO mice compared to wt controls.

3.6 | Less expression of phagocytosis-associated activatory membrane adaptors and lysosomal/endosomal Cd68 in TREM2 KO mice and decreased phagocytosis of TREM2 KO microglia

The phagocytic removal of debris and unwanted structures is necessary for normal brain homeostasis. During aging more debris, apoptotic cells and oxidized lipids might occur that have to be removed by the microglia. Our RNA-seq data hint toward differences in microglial phagocytosis in 24 months old TREM2 KO versus wt littermates since *Tyrobp* (*Dap12*), the adaptor molecule of TREM2, and the lysosomal/endosomal associated membrane glycoprotein *Cd68* belong to the DE genes (Supporting Information Figure S3A). To validate the RNA-seq data, we investigated the transcription levels of *Dap12*, *Fcer1g*, and *Cd68* over time that revealed genotype-specific differences in a multiple linear model (Figure 5a; *Dap12* $p < .0001$; *Fcer1g* $p = .0045$; *Cd68* $p = .0077$). Especially at 24 months of age, all three markers are transcribed less in the TREM2 KO mice compared to wt littermates (*Dap12* wt 1.32 ± 0.05 FC, KO 0.81 ± 0.06 FC, $p < .001$; *Fcer1g* wt 0.71 ± 0.03 FC, KO 0.47 ± 0.05 FC, $p < .001$; *Cd68* wt 1.05 ± 0.14 FC, KO 0.57 ± 0.09 FC, $p = .006$). Moreover, no age-related increase in the expression of the microglial phagocytosis marker Cd68 was observed in the TREM2 KO mice. The Iba1 stained coronal slices have been co-stained with an antibody directed against Cd68 (Figure 5b). In TREM2 KO mice, the relative overall intensity of Cd68 per area was decreasing with age (3 months vs. 24 months: $p = .001$), whereas the Cd68 intensity per Iba1-positive soma was stable (3 months vs. 24 months: $p = .078$), while both parameters were increasing in the wt littermate controls (Figure 5c; overall intensity 3 months vs. 12 months: $p = .022$; soma intensity 3 months v. 24 months: $p < .001$; genotype-specific differences: for both $p < .0001$). Especially in 24 months old animals, the relative overall Cd68 intensity per area (Figure 5c, *left*; wt 167.94 ± 27.18%, KO 55.47 ± 5.18%, $p < .001$) as well as the relative Cd68 soma intensity per area (Figure 5c, *right*; wt 311.27 ± 34.38%, KO 148.34 ± 15.34%, $p < .001$) was lower in TREM2 KO mice compared to wt littermates. To investigate the microglial phagocytic function in more detail, we analyzed the phagocytosis of beads (Figure 5d, *left*) as well as of inactivated bacteria (Figure 5d, *right*) of primary cultured microglia via flow cytometry or confocal microscopy, respectively. The relative beads phagocytosis as well as the phagocytosis of inactivated bacteria was lower in TREM2 KO compared to wt primary microglia (beads: wt 100 ± 14.7% and TREM2 KO 37.24 ± 5.06%, $p = .016$; inactivated bacteria: wt 100 ± 4.76%, TREM2 KO 63.11 ± 2.69%, $p < .001$).

Thus, the lower expression level of phagocytic markers in TREM2 KO mice as well as the decreased phagocytic capacity of TREM2 KO microglia further support the RNA-seq data indicating a lower phagocytic activation status.

4 | DISCUSSION

Several TREM2 mutations have been associated with age-related inflammatory neurodegenerative diseases. However, the exact role of TREM2 in the aging process of the brain is still unknown. Our data now demonstrate that TREM2 deficiency leads to less age-related neuronal loss. Already at 3 months of age, a slight increase in neuronal numbers in the SN as well as a slight increase in synapse density were detected in TREM2 KO compared to wt mice. While the neuronal cell number and the synapse density were preserved over time in TREM2 KO mice, both were reduced with age in the wt animals. This finding is in line with another previous observation from Leyns et al. (2017) investigating the impact of TREM2 on tau pathology. Loss of TREM2 in a tau mouse model led to less brain atrophy. Interestingly, deficiency of TYROBP, the adapter protein for TREM2, was neuroprotective in a mouse model of AD (Haure-Mirande et al., 2017). The deficiency of TYROBP resulted in an altered expression of AD-related genes, with less severe neuritic dystrophy and attenuated learning behavior deficits. Moreover, a current study indicates a role for TREM2 in synaptic pruning during brain development. In the developing brain, deficiency of TREM2 resulted in a higher density of synaptic structures that was attended by enhanced excitatory neurotransmission

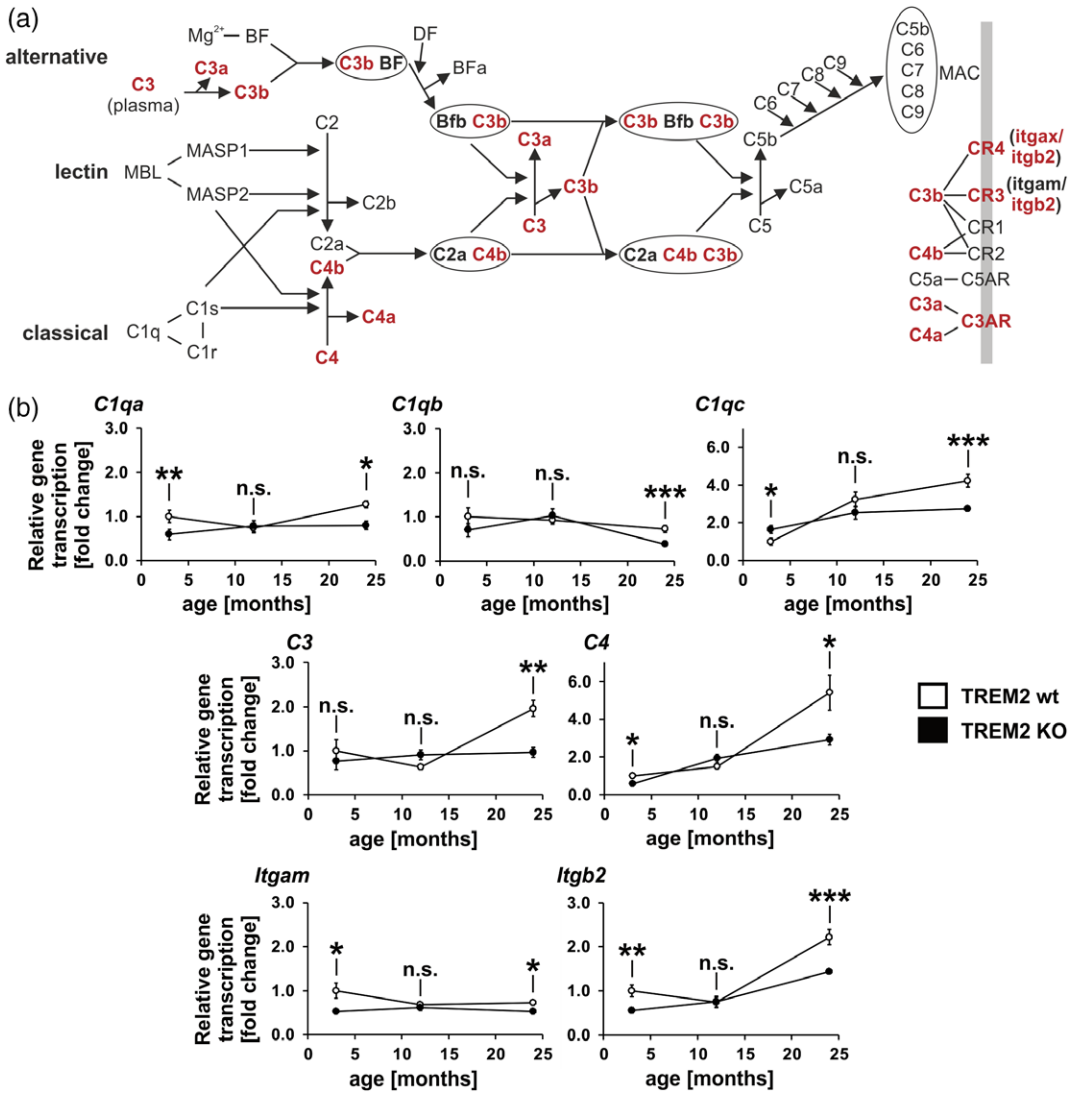

FIGURE 4 Less age-related increase in complement factors in TREM2 KO mice. (a) The complement pathway is less activated in 24 months old TREM2 knock-out (KO) animals. Significantly down-regulated genes are shown in red and bold. Protein names corresponding to differentially expressed (DE) genes are shown. Ingenuity pathway analysis was performed on significantly DE genes (FC > 0.5, FDR < 0.05). (b) Semi-quantitative real-time PCR of complement factors in half brain of 3, 12, and 24 months old TREM2 wild-type (wt) and KO. At 24 months of age transcription of complement components and parts of the complement receptor 3 (*Itgam*, *Itgb2*) was lower in TREM2 KO mice. *Gapdh* was used as internal loading control. Data are presented as mean ± SEM (n = 6–12 mice per group; *$p \leq .05$; **$p \leq .01$; ***$p \leq .001$; n.s. not significant)

and reduced long-range functional connectivity (Filipello et al., 2018). This might be due to the absence of TREM2-mediated phagocytosis. In our study, TREM2 KO mice have preserved neuronal numbers as well as an increased number of synaptic co-puncta. In line, we observed lower levels of phagocytic markers and decreased phagocytosis of TREM2 KO primary microglia. However, it still has to be clarified whether the preserved neuronal numbers have any functional impact. Another study in TREM2-deficient mice already demonstrated that TREM2 sustains microglial expansion during aging because 24 months old TREM2-deficient mice had fewer microglia in the corpus callosum, cerebellum and hippocampus (Poliani et al., 2015). Moreover, a further study showed that TREM2 promotes microglial survival in an AD mouse model (Wang et al., 2015). Consistently, our study demonstrated lower microglial density also in the SN of TREM2 KO mice accompanied by less pro-inflammatory cytokine, complement component, and microglial marker transcripts. The fact that TREM2 KO mice do not show an increased gene transcription of *Il-1β* and/or *Tnfα* after crossing with different AD mice (Jay et al., 2015; Wang et al., 2015) or after experimental stroke (Sieber et al., 2013) was already observed before. These initial findings were also recently elaborated by Mazaheri et al. (2017) and Krasemann et al. (2017). This was also confirmed recently in tau transgenic mice deficient for TREM2. The indicated animals displayed reduced microgliosis and lower levels of inflammatory cytokines (Leyns et al., 2017). Interestingly, also in an AD mouse model expressing the human AD-associated TREM2 R47H variant reduced microgliosis and less *Il-1β* gene transcription was observed compared to mice expressing the human common TREM2 variant (Song et al., 2018). Thus, data hint toward TREM2 being involved in the regulation of microglial numbers. In line, our data demonstrate that TREM2 KO mice have less gene transcription of complement factors. Recently, complement has been linked to age-related neurodegeneration. Complement C3-deficient

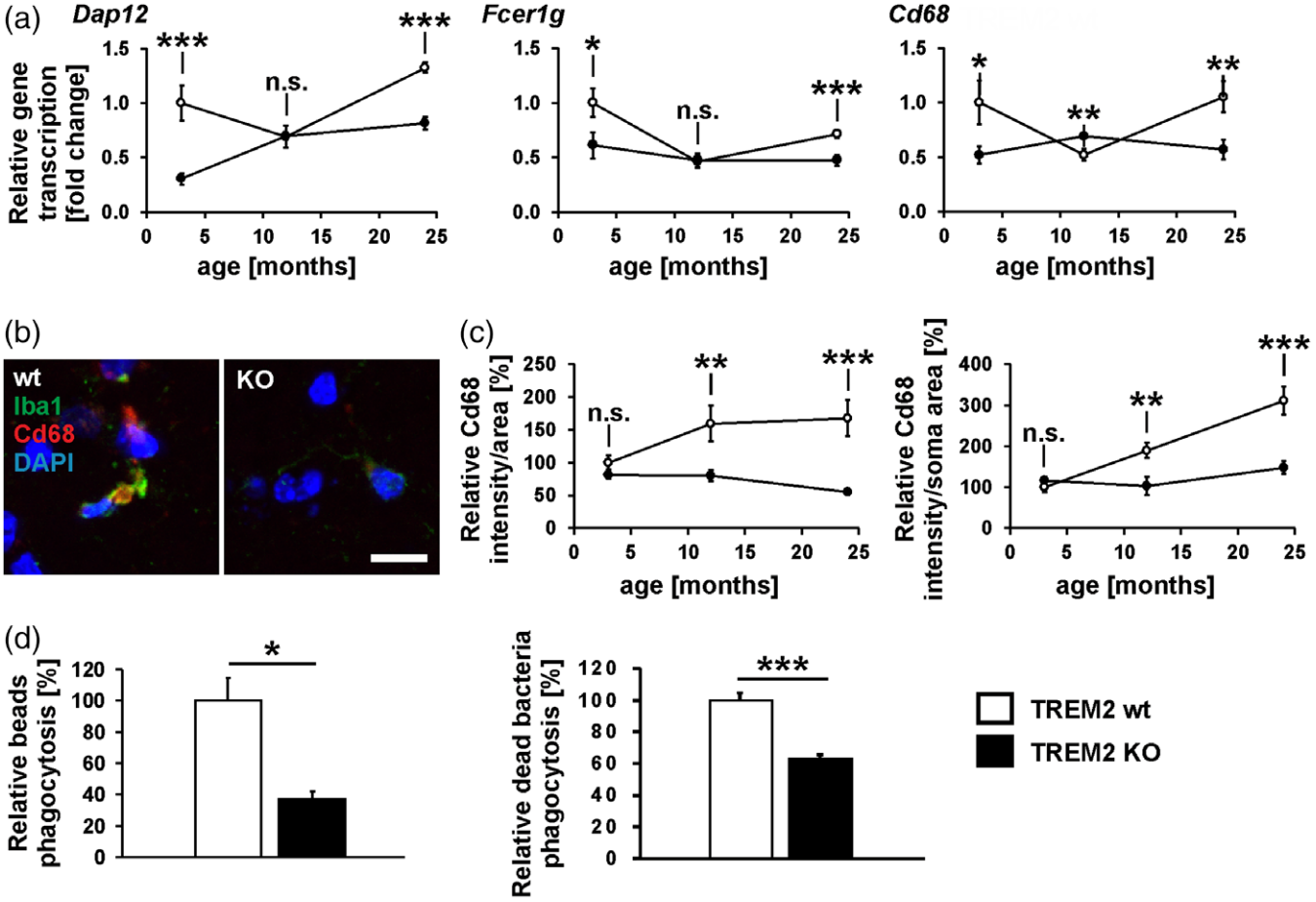

FIGURE 5 Less expression of phagocytosis-associated activatory membrane adaptors and Cd68 in TREM2 KO mice and decreased phagocytosis of TREM2 KO microglia. (a) Semi-quantitative real-time PCR of phagocytic markers in half brains of 3, 12, and 24 months old TREM2 wild-type (wt) and knock-out (KO) mice. At 24 months of age transcription of *Dap12*, *Fcer1g* (fc receptor gamma), and *Cd68* was lower in TREM2 KO mice. *Gapdh* was used as internal loading control. (b) Representative z-stack images of ionized calcium binding adaptor molecule 1 (Iba1, green), Cd68 (red), and 4′,6-diamidin-2-phenylindole (DAPI, blue) staining in the substantia nigra *pars reticulata* (SN*pr*) in 24 months old TREM2 wild-type (wt) and knock-out (KO) animals. Scale bar: 10 μm; Bregma level: −2.90 mm. (c) Quantification of whole Cd68 staining intensity per area (*left*) and Cd68 staining intensity per Iba1-positive cell soma area (*right*) revealed no age-related increase in Cd68 staining intensities in TREM2 KO animals. Especially, at 24 months of age, the whole Cd68 staining intensity as well as the Cd68 intensity of the soma are lower in TREM2 KO mice. (d) Analysis of beads phagocytosis by flow cytometry (*left*) and pHrodo-inactivated bacteria phagocytosis by confocal microscopy (*right*) in primary microglia obtained from TREM2 wt and KO mice. Quantification of phagocytic activity showed reduced phagocytosis of beads as well as inactivated bacteria by primary microglia from TREM2 KO mice. Data are presented as mean + *SEM* or mean ± *SEM* (n = 5–12 mice per group (a-c) and n = 3 independent culture preparations (d). *$p \leq .05$; **$p \leq .01$; ***$p \leq .001$; n.s. not significant)

mice failed to display an age-related hippocampal decline in the typical aging process (Shi et al., 2015) and displayed less neurodegeneration in aged AD model mice (Shi et al., 2017). Thus, decreased loss of neurons in TREM2 KO mice possibly might be related to the reduced complement expression. That loss of TREM2 keeps microglia in a less activated status is also confirmed by our results hinting toward less oxidative stress in brains of aged TREM2 KO mice. Upon ligand binding, TREM2 activates downstream protein tyrosine phosphorylation through its adaptor TYROBP and can signal toward phagocytosis and production of ROS (Charles et al., 2008; N'Diaye et al., 2009; Zhu, Li, Wu, Huang, & Wu, 2014). We now observed less staining of oxidized lipids as well as a reduced oxidative burst of debris- or inactivated bacteria-challenged cultured microglia of TREM2 KO mice. Primary microglia from neonatal mice are not reflecting the situation of an aging brain. However, whether TREM2 contributes to the production of radicals has not been investigated so far. With the well-established procedure of primary microglia, we got the first hint, indicating that TREM2 might be involved in accumulation of oxidized lipids possibly via its capacity to produce ROS.

Our data demonstrating that loss of TREM2 in mice leads to lower microglial density accompanied by less inflammatory gene transcription and less oxidative stress appears to be contrary to what has been observed in NHD patients. Loss-of-function of TREM2 or TYROBP in NHD is associated with the upregulation of genes involved in the inflammatory response (Numasawa et al., 2011) and the expression of the ROS producing NADPH oxidase subunit gp91phox in microglia; suggesting a disease-relevant ROS-mediated white matter damage (Satoh et al., 2016). Age (decades in humans versus 24 months in mice) and/or environmental triggers (infections in humans vs. specific-pathogen-free [SPF]-housing of mice) might contribute to these substantial differences. Furthermore, microglial cells are highly plastic and can polarize toward different phenotypes.

Recently, it has been shown in mice that a small microglial subpopulation can completely switch toward a neurodegenerative disease-associated phenotype when triggered by local environmental factors (Keren-Shaul et al., 2017). TREM2 appears to be a master regulator of the microglial switch toward a neurotoxic phenotype in mice (Keren-Shaul et al., 2017; Krasemann et al., 2017) and in parallel can restrict the over-shooting inflammatory cytokine production induced by pattern recognition receptors (Hamerman et al., 2006; Turnbull et al., 2006). In aged humans, the chronic neurodegenerative disease-associated microglia can have an activated, lipid-loaded, CD68+, MHC class II+, and dystrophic phenotype (Streit, Xue, Tischer, & Bechmann, 2014; Tischer et al., 2016), thus indicating a phenotypic microglial switch. However, we failed to observe such a phenotypic microglial switch in mice, possibly because the TREM2 KO mice were housed in an SPF animal facility, driving the microglia to remain locked in the homeostatic status for the entire life-span of the animals.

In conclusion, our data show that TREM2 impacts the amount of microglia and therewith the inflammatory status of the brain, as well as the neuronal numbers and synaptic co-puncta during physiological aging.

ACKNOWLEDGMENTS

The authors thank Rita Jietou and Sharon Weingarten for excellent technical support. This project was supported by the Deutsche Forschungsgemeinschaft DFG-LI 2833/1-1, DFG-SFB704, DFG-ImmunoSensation-EXC1023 and the Hertie-Foundation. HN and JW have received funding from the Innovative Medicines Initiative 2 Joint Undertaking under grant agreement No 115976 (PHAGO). The RNA-seq analysis was carried out using the HPC (High-Performance Computing) facilities of the Université du Luxembourg (Varrette, Bouvry, Cartiaux, & Georgatos, 2014).

CONFLICT OF INTEREST

The authors have no conflicting financial interests.

ORCID

Harald Neumann https://orcid.org/0000-0002-5071-5202

REFERENCES

Beutner, C., Roy, K., Linnartz, B., Napoli, I., & Neumann, H. (2010). Generation of microglial cells from mouse embryonic stem cells. *Nature Protocols*, *5*(9), 1481–1494. https://doi.org/10.1038/nprot.2010.90

Bianchin, M. M., Martin, K. C., de Souza, A. C., de Oliveira, M. A., & Rieder, C. R. (2010). Nasu-Hakola disease and primary microglial dysfunction. *Nature Reviews. Neurology*, *6*(9),523. doi:https://doi.org/10.1038/nrneurol.2010.17-c1

Cannon, J. P., O'Driscoll, M., & Litman, G. W. (2012). Specific lipid recognition is a general feature of CD300 and TREM molecules. *Immunogenetics*, *64*(1), 39–47. https://doi.org/10.1007/s00251-011-0562-4

Charles, J. F., Humphrey, M. B., Zhao, X., Quarles, E., Nakamura, M. C., Aderem, A., … Smith, K. D. (2008). The innate immune response to salmonella enterica serovar typhimurium by macrophages is dependent on TREM2-DAP12. *Infection and Immunity*, *76*(6), 2439–2447. https://doi.org/10.1128/IAI.00115-08

Claude, J., Linnartz-Gerlach, B., Kudin, A. P., Kunz, W. S., & Neumann, H. (2013). Microglial CD33-related Siglec-E inhibits neurotoxicity by preventing the phagocytosis-associated oxidative burst. *The Journal of Neuroscience*, *33*(46), 18270–18276. https://doi.org/10.1523/JNEUROSCI.2211-13.2013

Daws, M. R., Sullam, P. M., Niemi, E. C., Chen, T. T., Tchao, N. K., & Seaman, W. E. (2003). Pattern recognition by TREM-2: Binding of anionic ligands. *Journal of Immunology*, *171*(2), 594–599.

Filipello, F., Morini, R., Corradini, I., Zerbi, V., Canzi, A., Michalski, B., … Matteoli, M. (2018). The microglial innate immune receptor TREM2 is required for synapse elimination and Normal brain connectivity. *Immunity*, *48*(5), 979–991 e978. https://doi.org/10.1016/j.immuni.2018.04.016

Guerreiro, R., Wojtas, A., Bras, J., Carrasquillo, M., Rogaeva, E., Majounie, E., … Alzheimer Genetic Analysis, G. (2013). TREM2 variants in Alzheimer's disease. *The New England Journal of Medicine*, *368*(2), 117–127. https://doi.org/10.1056/NEJMoa1211851

Hamerman, J. A., Jarjoura, V. R., Humphrey, M. B., Nakamura, A. C., Seaman, W. E., & Lanier, L. L. (2006). Cutting edge: Inhibition of TLR and FcR responses in macrophages by triggering receptor expressed on myeloid cells (TREM)-2 and DAP12. *Journal of Immunology*, *177*(4), 2051–2055. https://doi.org/10.4049/jimmunol.177.4.2051

Haure-Mirande, J. V., Audrain, M., Fanutza, T., Kim, S. H., Klein, W. L., Glabe, C., … Ehrlich, M. E. (2017). Deficiency of TYROBP, an adapter protein for TREM2 and CR3 receptors, is neuroprotective in a mouse model of early Alzheimer's pathology. *Acta Neuropathologica*, *134*(5), 769–788. https://doi.org/10.1007/s00401-017-1737-3

Ippolito, D. M., & Eroglu, C. (2010). Quantifying synapses: An immunocytochemistry-based assay to quantify synapse number. *Journal of Visualized Experiments*, *45*. https://doi.org/10.3791/2270

Jay, T. R., Miller, C. M., Cheng, P. J., Graham, L. C., Bemiller, S., Broihier, M. L., … Lamb, B. T. (2015). TREM2 deficiency eliminates TREM2+ inflammatory macrophages and ameliorates pathology in Alzheimer's disease mouse models. *The Journal of Experimental Medicine*, *212*(3), 287–295. https://doi.org/10.1084/jem.20142322

Jonsson, T., Stefansson, H., Steinberg, S., Jonsdottir, I., Jonsson, P. V., Snaedal, J., … Stefansson, K. (2013). Variant of TREM2 associated with the risk of Alzheimer's disease. *The New England Journal of Medicine*, *368*(2), 107–116. https://doi.org/10.1056/NEJMoa1211103

Keren-Shaul, H., Spinrad, A., Weiner, A., Matcovitch-Natan, O., Dvir-Szternfeld, R., Ulland, T. K., … Amit, I. (2017). A unique microglia type associated with restricting development of Alzheimer's disease. *Cell*, *169*(7), 1276–1290. https://doi.org/10.1016/j.cell.2017.05.018

Kierdorf, K., Erny, D., Goldmann, T., Sander, V., Schulz, C., Perdiguero, E. G., … Prinz, M. (2013). Microglia emerge from erythromyeloid precursors via Pu.1- and Irf8-dependent pathways. *Nature Neuroscience*, *16*(3), 273–280. https://doi.org/10.1038/nn.3318

Kober, D. L., Alexander-Brett, J. M., Karch, C. M., Cruchaga, C., Colonna, M., Holtzman, M. J., & Brett, T. J. (2016). Neurodegenerative disease mutations in TREM2 reveal a functional surface and distinct loss-of-function mechanisms. *eLife*, *5*, e20391. https://doi.org/10.7554/eLife.20391

Krasemann, S., Madore, C., Cialic, R., Baufeld, C., Calcagno, N., El Fatimy, R., … Butovsky, O. (2017). The TREM2-APOE pathway drives the transcriptional phenotype of dysfunctional microglia in neurodegenerative diseases. *Immunity*, *47*(3), 566–581. https://doi.org/10.1016/j.immuni.2017.08.008

Leyns, C. E. G., Ulrich, J. D., Finn, M. B., Stewart, F. R., Koscal, L. J., Remolina Serrano, J., … Holtzman, D. M. (2017). TREM2 deficiency attenuates neuroinflammation and protects against neurodegeneration in a mouse model of tauopathy. *Proceedings of the National Academy of Sciences of the United States of America*, *114*(43), 11524–11529. https://doi.org/10.1073/pnas.1710311114

Mazaheri, F., Snaidero, N., Kleinberger, G., Madore, C., Daria, A., Werner, G., … Haass, C. (2017). TREM2 deficiency impairs chemotaxis and microglial responses to neuronal injury. *EMBO Reports*, *18*(7), 1186–1198. https://doi.org/10.15252/embr.201743922

Napoli, I., Kierdorf, K., & Neumann, H. (2009). Microglial precursors derived from mouse embryonic stem cells. *Glia*, *57*(15), 1660–1671. https://doi.org/10.1002/glia.20878

N'Diaye, E. N., Branda, C. S., Branda, S. S., Nevarez, L., Colonna, M., Lowell, C., … Seaman, W. E. (2009). TREM-2 (triggering receptor expressed on myeloid cells 2) is a phagocytic receptor for bacteria. *The Journal of Cell Biology*, *184*, 215–223. https://doi.org/10.1083/jcb.200808080

Numasawa, Y., Yamaura, C., Ishihara, S., Shintani, S., Yamazaki, M., Tabunoki, H., & Satoh, J. I. (2011). Nasu-Hakola disease with a splicing mutation of TREM2 in a Japanese family. *European Journal of Neurology*, *18*(9), 1179–1183. https://doi.org/10.1111/j.1468-1331.2010.03311.x

Otero, K., Shinohara, M., Zhao, H., Cella, M., Gilfillan, S., Colucci, A., … Colonna, M. (2012). TREM2 and beta-catenin regulate bone homeostasis by controlling the rate of osteoclastogenesis. *Journal of Immunology*, *188*(6), 2612–2621. https://doi.org/10.4049/jimmunol.1102836

Paloneva, J., Kestila, M., Wu, J., Salminen, A., Bohling, T., Ruotsalainen, V., … Peltonen, L. (2000). Loss-of-function mutations in TYROBP (DAP12) result in a presenile dementia with bone cysts. *Nature Genetics*, *25*, 357–361. https://doi.org/10.1038/77153

Paloneva, J., Manninen, T., Christman, G., Hovanes, K., Mandelin, J., Adolfsson, R., … Peltonen, L. (2002). Mutations in two genes encoding different subunits of a receptor signaling complex result in an identical disease phenotype. *American Journal of Human Genetics*, *71*(3), 656–662. https://doi.org/10.1086/342259

Poliani, P. L., Wang, Y., Fontana, E., Robinette, M. L., Yamanishi, Y., Gilfillan, S., & Colonna, M. (2015). TREM2 sustains microglial expansion during aging and response to demyelination. *The Journal of Clinical Investigation*, *125*(5), 2161–2170. https://doi.org/10.1172/JCI77983

Satoh, J. I., Kino, Y., Yanaizu, M., Tosaki, Y., Sakai, K., Ishida, T., & Saito, Y. (2016). Expression of gp91phox and p22phox, catalytic subunits of NADPH oxidase, on microglia in Nasu-Hakola disease brains. *Intractable & Rare Diseases Research*, *5*(4), 275–279. https://doi.org/10.5582/irdr.2016.01086

Schlepckow, K., Kleinberger, G., Fukumori, A., Feederle, R., Lichtenthaler, S. F., Steiner, H., & Haass, C. (2017). An Alzheimer-associated TREM2 variant occurs at the ADAM cleavage site and affects shedding and phagocytic function. *EMBO Molecular Medicine*, *9*(10), 1356–1365. https://doi.org/10.15252/emmm.201707672

Shi, Q., Chowdhury, S., Ma, R., Le, K. X., Hong, S., Caldarone, B. J., … Lemere, C. A. (2017). Complement C3 deficiency protects against neurodegeneration in aged plaque-rich APP/PS1 mice. *Science Translational Medicine*, *9*(392), eaaf6295. https://doi.org/10.1126/scitranslmed.aaf6295

Shi, Q., Colodner, K. J., Matousek, S. B., Merry, K., Hong, S., Kenison, J. E., … Lemere, C. A. (2015). Complement C3-deficient mice fail to display age-related hippocampal decline. *The Journal of Neuroscience*, *35*(38), 13029–13042. https://doi.org/10.1523/JNEUROSCI.1698-15.2015

Sieber, M. W., Jaenisch, N., Brehm, M., Guenther, M., Linnartz-Gerlach, B., Neumann, H., … Frahm, C. (2013). Attenuated inflammatory response in triggering receptor expressed on myeloid cells 2 (TREM2) Knock-out mice following stroke. *PLoS One*, *8*(1), e52982. https://doi.org/10.1371/journal.pone.0052982

Song, W. M., Joshita, S., Zhou, Y., Ulland, T. K., Gilfillan, S., & Colonna, M. (2018). Humanized TREM2 mice reveal microglia-intrinsic and -extrinsic effects of R47H polymorphism. *The Journal of Experimental Medicine*, *215*(3), 745–760. https://doi.org/10.1084/jem.20171529

Streit, W. J., Xue, Q. S., Tischer, J., & Bechmann, I. (2014). Microglial pathology. *Acta Neuropathologica Communications*, *2*, 142. https://doi.org/10.1186/s40478-014-0142-6

Takahashi, K., Rochford, C. D. P., & Neumann, H. (2005). Clearance of apoptotic neurons without inflammation by microglial triggering receptor expressed on myeloid cells-2. *Journal of Experimental Medicine*, *201*(4), 647–657. https://doi.org/10.1084/jem.20041611

Thornton, P., Sevalle, J., Deery, M. J., Fraser, G., Zhou, Y., Stahl, S., … Crowther, D. C. (2017). TREM2 shedding by cleavage at the H157-S158 bond is accelerated for the Alzheimer's disease-associated H157Y variant. *EMBO Molecular Medicine*, *9*(10), 1366–1378. https://doi.org/10.15252/emmm.201707673

Tischer, J., Krueger, M., Mueller, W., Staszewski, O., Prinz, M., Streit, W. J., & Bechmann, I. (2016). Inhomogeneous distribution of Iba-1 characterizes microglial pathology in Alzheimer's disease. *Glia*, *64*(9), 1562–1572. https://doi.org/10.1002/glia.23024

Turnbull, I. R., Gilfillan, S., Cella, M., Aoshi, T., Miller, M., Piccio, L., … Colonna, M. (2006). Cutting edge: TREM-2 attenuates macrophage activation. *Journal of Immunology*, *177*(6), 3520–3524. https://doi.org/10.4049/jimmunol.177.6.3520

Varrette, S., Bouvry, P., Cartiaux, H., & Georgatos, F. (2014). *Management of an academic HPC cluster: The UL experience*. In: Proceedings of the 2014 International Conference on High Performance Computing and Simulation (HPCS 2014), Bologna, Italy, pp. 959–967. IEEE, July 2014. doi:https://doi.org/10.1109/HPCSim.2014.6903792

Wang, Y., Cella, M., Mallinson, K., Ulrich, J. D., Young, K. L., Robinette, M. L., … Colonna, M. (2015). TREM2 lipid sensing sustains the microglial response in an Alzheimer's disease model. *Cell*, *160*(6), 1061–1071. https://doi.org/10.1016/j.cell.2015.01.049

Zhu, M., Li, D., Wu, Y., Huang, X., & Wu, M. (2014). TREM-2 promotes macrophage-mediated eradication of Pseudomonas aeruginosa via a PI3K/Akt pathway. *Scandinavian Journal of Immunology*, *79*(3), 187–196. https://doi.org/10.1111/sji.12148

SUPPORTING INFORMATION

Additional supporting information may be found online in the Supporting Information section at the end of the article.

How to cite this article: Linnartz-Gerlach B, Bodea L-G, Klaus C, et al. TREM2 triggers microglial density and age-related neuronal loss. *Glia*. 2018;1–12. https://doi.org/10.1002/glia.23563